Shifting microbial communities sustain multi-year iron reduction and methanogenesis in ferruginous sediment incubations

Marcus S. Bray[1], Jieying Wu[1], Benjamin C. Reed[1], Cecilia B. Kretz[2], Rachel L. Simister[3], Cynthia Henny[4], Frank J. Stewart[1,2], Thomas J. DiChristina[1,2], Jay A. Brandes[5], David A. Fowle[6], Sean A. Crowe[3], Jennifer B. Glass[1,2#]

[1]School of Biology, Georgia Institute of Technology, Atlanta, GA, 30332, USA

[2]School of Earth and Atmospheric Sciences, Georgia Institute of Technology, Atlanta, GA, 30332, USA

[3]Departments of Microbiology & Immunology and Earth, Ocean, & Atmospheric Sciences, University of British Columbia, Vancouver, BC, Canada

[4]Research Center for Limnology, Indonesian Institute of Sciences, Cibinong, Indonesia

[5]Skidaway Institute of Oceanography, Savannah, GA, 31411, USA

[6]Department of Geology, University of Kansas, Lawrence, KS, 66045, USA

[#]Correspondence: 311 Ferst Drive Atlanta, GA; Telephone: 404-894-3942; Fax: 404-894-5638; Email: Jennifer.Glass@eas.gatech.edu

Type: Research Article

Abstract

Reactive Fe^{3+} minerals can influence methane (CH_4) emissions by inhibiting microbial methanogenesis or by stimulating anaerobic CH_4 oxidation. The balance between Fe^{3+} reduction, methanogenesis, and methane oxidation in the ferruginous Archean oceans would have controlled CH_4 fluxes to the atmosphere, thereby regulating the capacity for CH_4 to warm the early Earth under the Faint Young Sun. We studied CH_4 and Fe cycling in anoxic incubations of ferruginous sediment from the Archean ocean analogue Lake Matano, Indonesia over three successive transfers (500 days total). Iron reduction, methanogenesis, methane oxidation, and microbial taxonomy were monitored in treatments amended with 10 mM ferrihydrite or goethite. After three dilutions, Fe^{3+} reduction persisted only in bottles with ferrihydrite. Enhanced CH_4 production was observed in the presence of goethite. Methane oxidation was observed throughout incubations, although stoichiometry suggested that Fe^{3+} was not the sole electron acceptor. 16S rRNA profiles continuously changed over the course of enrichment, with ultimate dominance of unclassified members of the order Desulfuromonadales in all treatments and Rhodocyclaceae in treatments amended with CH_4. Microbial diversity decreased markedly over the course of incubation, with subtle differences being observed between ferrihydrite and goethite. These results suggest that Fe^{3+}-oxide mineralogy and availability of electron donors could have led to spatial separation of Fe^{3+}-reducing and methanogenic microbial communities in ancient ferruginous marine sediments, potentially explaining the persistence of CH_4 as a greenhouse gas throughout the Archean.

INTRODUCTION

Anoxic and ferruginous conditions were common in Archean oceans (Poulton & Canfield, 2011). In Archean seawater, Fe would have undergone extensive redox cycling via microbial photoferrotrophy or abiotic photo-oxidation of dissolved Fe^{2+} to Fe^{3+} followed by microbial respiration of Fe^{3+} to Fe^{2+} (Kappler et al., 2005 ; Crowe et al., 2008a ; Konhauser et al., 2005). Indeed, Fe^{3+} reduction evolved early in Earth's history (Craddock & Dauphas, 2011 ; Johnson et al., 2008) and may have contributed extensively to organic matter oxidation in the Archean (Vargas et al., 1998).

Elevated atmospheric methane (CH_4; 100-1000 ppmv in the Archean vs. ~2 ppmv in the modern atmosphere) could have played a role in the Archean greenhouse effect that sustained temperatures warm enough for liquid water under considerably lower solar radiation (Pavlov et al., 2000 ; Haqq-Misra et al., 2008 ; Kasting, 2005). The source of Archean CH_4 was likely hydrogenotrophic methanogenesis ($CO_2 + 4\ H_2 \rightarrow CH_4 + 2H_2O$; (Ueno et al., 2006 ; Battistuzzi et al., 2004). However, this form of methanogenesis typically yields minimal free energy and is outcompeted by metal-reducing organisms with a higher affinity for H_2 than methanogens in the presence of poorly crystalline Fe^{3+} (e.g. ferrihydrite; Lovley & Phillips, 1987 ; Lovley & Goodwin, 1988 ; Zhou et al., 2014). Ferrihydrite reduction can also outcompete acetoclastic methanogenesis ($CH_3COO^- + H^+ \rightarrow CH_4 + CO_2$) due to the higher affinity for acetate (CH_3COO^-) by Fe^{3+}-reducing bacteria compared to methanogens (Lovley & Phillips, 1986), although acetoclastic methanogenesis likely evolved late in Earth's history (Fournier & Gogarten, 2008). Ferruginous oceans would have further suppressed CH_4 emissions if Fe^{3+} played a role in supplying electron acceptors for CH_4 oxidation, either as the direct oxidant, or indirectly through the regeneration of sulfate through oxidation of reduced sulfur compounds (Sivan et al., 2014).

Methane oxidation coupled directly to Fe^{3+} reduction is thermodynamically favorable according to the free energy yield with ferrihydrite ($CH_4 + 8\ Fe(OH)_3 + 15H^+ \rightarrow HCO_3^- + 8Fe^{2+} + 21H_2O$; ΔG_r^0 = -571 kJ mol^{-1} CH_4) and goethite ($CH_4 + 8\ FeOOH + 15H^+ \rightarrow HCO_3^- + 8Fe^{2+} + 13H_2O$; ΔG_r^0 = -355 kJ mol^{-1} CH_4) as terminal electron acceptors. We would expect to observe a stoichiometric ratio of 1 CH_4 oxidized per 8 Fe^{3+} reduced and, based on energetic yields, the preferential use of ferrihydrite over goethite as the electron acceptor in this putative metabolism. In addition, accumulating geochemical evidence for microbial CH_4 oxidation coupled to, or stimulated by, Fe^{3+} reduction is widespread across modern anoxic ecosystems and anaerobic digester communities (Sivan et al., 2011 ; Segarra et al., 2013 ; Beal et al., 2009 ; Amos et al., 2012 ; Riedinger et al., 2014 ; Noroi et al., 2013 ; Crowe et al., 2011 ; Sturm et al., 2015 ; Egger et al., 2015 ; Zehnder & Brock, 1980 ; Sivan et al., 2014 ; Fu et al., 2016 ; Rooze et al., 2016). However, robust and direct evidence for this putative metabolism in the form of stable enrichment cultures or microbial isolates remains elusive.

Despite the possible importance of coupled Fe and CH_4 cycling in the Archean Eon, long-term studies of Fe^{3+} reduction under low organic carbon and high CH_4 conditions remain sparse. Lake Matano, Indonesia is one of the only modern analogues for the ferruginous Archean oceans (Crowe et al., 2008a). Despite the presence of Fe^{3+} oxides that might be expected to suppress methanogenesis, CH_4 accumulates to 1.4 mM in anoxic deep waters (Crowe et al., 2008a ; Crowe et al., 2011 ; Crowe et al., 2008b ; Crowe et al., 2007). Methanotrophy is a key carbon fixation process in Lake Matano's oxic-anoxic transition zone, and the dearth of other oxidants (<100 nM nitrate and sulfate) suggests that Fe^{3+} might be the primary electron acceptor in methanotrophy (Sturm et al., 2015 ; Crowe et al., 2011). In this study, we examined the influence of CH_4 and Fe^{3+} mineral speciation on CH_4 and Fe biogeochemistry together with

87 microbial community composition over three successive dilutions (500 total days of incubation)
88 of anoxic Lake Matano sediments.
89
90 ## MATERIALS AND METHODS
91
92 ### Sample collection and storage
93 A 15-cm sediment core from 200 m water depth in Lake Matano, Sulawesi Island, Indonesia
94 (2°26′S, 121°15′E; *in situ* sediment temperature ~27°C) was sampled in November 2010 and
95 sub-sampled at 5 cm increments. Sediments from 0-5 and 5-10 cm depth were fluffy and black,
96 and 10-15 cm was dark gray. Sediments were sealed in gas-tight bags with no headspace
97 (Hansen et al., 2000) and stored at 4°C until incubations began in March 2015.
98
99 ### Enrichment medium and substrate synthesis
100 A modified artificial freshwater medium lacking nitrate and sulfate was developed based on the
101 pore water composition of Lake Matano sediments (S.A. Crowe and D.A. Fowle, unpublished
102 work). The medium contained 825 μM $MgCl_2$, 550 μM $CaCO_3$, 3 mM $NaHCO_3$, 3.5 μM
103 K_2HPO_4, 5 μM Na_2HPO_4, 225 μM NH_4Cl, 1 μM $CuCl_2$, 1.5 μM Na_2MoO_4, 2.5 μM $CoCl_2$, 23
104 μM $MnCl_2$, 4 μM $ZnCl_2$, 9.4 μM $FeCl_3$ and 3 mM Na_2NTA, 0.07 μM vitamin B_{12}, 0.4 μM biotin,
105 and 68.5 μM thiamine. Filter-sterilized vitamin solutions were added after autoclaving.
106 Ferrihydrite ($Fe(OH)_3$) and goethite (FeOOH) were synthesized as described in Schwertmann &
107 Cornell (1991) and added to enrichments to 10 mM as described below.
108
109 ### Inoculation of enrichment and amendments

The sediment was pre-treated for 36 days at 30°C in 100% N_2 headspace to deplete endogenous organic carbon, electron donors, and reactive electron acceptors. After pre-treatment, sediment from the 0-5 cm depth layer was inoculated in a ratio of sediment to medium of 1:5 (v/v) in an anoxic chamber (97% N_2 and 3% H_2; Coy Laboratory Products, Grass Lake, MI, USA). Sediment slurry (35 mL) was aliquoted into 70 mL sterile serum bottles, stoppered with sterile butyl stoppers (Geo-Microbial Technologies, Ochelata, OK, USA; pre-boiled in 0.1 N NaOH), and crimped with aluminum seals. Ferric iron was added either as ferrihydrite or goethite to 10 mM. Bottles were purged with 99.99% N_2 for 1 hr, and CH_4 amendments were injected with 10 mL 99.99% CH_4 and 5 mL 99% $^{13}CH_4$ (Cambridge Isotope Laboratories, Tewksbury, MA, USA). Controls were autoclaved at 121°C for 1 hr on day 0 and again on day 6 of the 1° enrichment. All treatments were duplicated, and bottles were incubated in the dark at 30°C with shaking at 200 rpm.

After 50 days, the volume of all cultures was reduced to 5 mL, and 30 mL of fresh media was added to each bottle, constituting a 6-fold dilution. These 2° enrichments were amended with an additional 10 mM of either ferrihydrite or goethite. All bottles were purged with 99.99% N_2 for 1 hr, and all bottles except N_2 controls were injected with 8 mL 99.99% CH_4 and 2 mL 99% $^{13}CH_4$. Controls were autoclaved again at 121°C for 1 hr. DL-Methionine (10 μM) was added as a sulfur source. After 303 days, cultures were diluted 10-fold with fresh media into new serum bottles (3° enrichment) with the same substrate and headspace composition as the 2° enrichment. A schematic of the incubation and dilutions is shown at the top of Figures 1-3.

HCl-extractable Fe^{2+} and Fe^{3+} and soluble Fe^{2+}

Samples were taken from each bottle in the anoxic chamber using a 22-gauge needle and plastic syringe. Plasticware was stored in the anoxic chamber for at least 24 hr to minimize O_2 sample contamination. For HCl-extractable Fe^{2+} analyses, 100 µL of sediment slurry was extracted with 400 µL 0.5 N HCl in the dark for 1 hr, followed by centrifugation at 10,000 x g for 1 min, injection of 10 µL of supernatant into 990 µL of 10 mM FerroZine reagent in 46 mM HEPES (pH 8.3), and measurement of absorbance at 562 nm (Stookey, 1970). For HCl-extractable Fe^{3+}, 100 µL of sediment slurry was incubated overnight in 0.5 N HCl and 0.25 M NH_2OH-HCl in the dark, followed by centrifugation and measurement as above, and subtraction of HCl-extractable Fe^{2+} as in Kostka & Luther (1994).

Methane oxidation

Samples were collected for δ^{13}C-DIC analysis by 0.2 µm membrane filtration of medium into crimp top autosampler vials (Thermo Scientific National Target LoVial) and analysis as described in Brandes (2009). Rates of $^{13}CH_4$ oxidation to ^{13}C-DIC were calculated over the linear period of δ^{13}C-DIC increase based on the method in Scheller et al. (2016). First, the δ^{13}C-DIC values were converted into fractional abundances ($^{13}F = (^{13}C/^{12}C+^{13}C)$), and then DIC production from CH_4 oxidation was calculated using the following formula:

$$\Delta[DIC] = ([DIC]_n(^{13}F_n)) - ([DIC]_0(13F_0))/^{13}F_{CH4})$$

Where $[DIC]_n$ and $^{13}F_n$ are equal to the total DIC concentration (mM) and fractional abundance of ^{13}C in the DIC at time n respectively. $[DIC]_0$ and $^{13}F_0$ are the total DIC concentration (mM) and fractional abundance of DIC at time 0 respectively, and $^{13}F_{CH4}$ is the fractional abundance of ^{13}C in the CH_4.

155 **Methane in headspace**

156 Headspace (50 µL) was sampled using a gastight syringe and injected into a gas chromatograph
157 (SRI Instruments 8610C, Torrance, CA, USA) with a HayeSep N column and flame ionization
158 detector to measure headspace CH_4 concentrations. A CH_4 standard (1000 ppm, Airgas, USA)
159 was used for calibration.

160

161 **16S rRNA gene amplicon sequencing**

162 Samples (2 mL) of sediment used for inoculating incubations (hereafter, "sediment inoculum")
163 were taken in February 2015 (prior to pre-treatment) and after incubation for 15 days (1°
164 enrichment), 72 days (2° enrichment) and 469 days (3° enrichment). Nucleic acid was extracted
165 and purified using a PowerSoil Isolation Kit following the manufacturer's protocol (Catalog #
166 12888; MO BIO, Carlsbad, CA, USA) and UltraClean® 15 Purification Kit (MO BIO
167 Laboratories, Carlsbad, CA). 16S rRNA gene amplicons were synthesized from extracted DNA
168 with V4 region-specific barcoded primers F515 and R806 (Caporaso et al., 2011) appended with
169 Illumina-specific adapters according to Kozich et al. (2013) using a C1000 Touch Thermocycler
170 (Bio-Rad, Hercules, CA) and QIAGEN Taq PCR Master Mix (QIAGEN, Venlo, Netherlands).
171 Thermal cycling conditions were as follows: initial denaturing at 94°C (5 min), 35 cycles of
172 denaturing at 94°C (40 sec), primer annealing at 55°C (40 sec), and primer extension at 68°C (30
173 sec). Amplicons were checked for correct size (~400 bp) on a 1% agarose gel and purified using
174 Diffinity RapidTips (Diffinity Genomics, West Henrietta, NY, USA). Amplicon concentrations
175 were determined fluorometrically on a Qubit™ (ThermoFisher Scientific, Waltham,
176 Massachusetts, USA). Amplicons were pooled at equimolar concentrations (4 nmol), and
177 sequenced on an Illumina MiSeq running MiSeq Control software v.2.4.0.4 using a 500 cycle

MiSeq reagent kit v2 with a 5% PhiX genomic library control, as described by Kozich et al. (2013). Sequences were deposited as NCBI accession numbers SAMN04532568-04532641 and SAMN05915184-05915222.

16S rRNA gene amplicon sequence analysis

Demultiplexed amplicon read pairs were quality trimmed with Trim Galore (Babraham Bioinformatics) using a base Phred33 score threshold of Q25 and a minimum length cutoff of 100 bp. Reads were then analyzed using mothur (Schloss et al., 2009) following its MiSeq standard operating procedure. High quality paired reads were merged and screened to remove sequences of incorrect length and those with high numbers of ambiguous base calls. Merged reads were dereplicated and aligned to the ARB SILVA database (release 123; available at http://www.mothur.org/wiki/Silva_reference_alignment). Sequences with incorrect alignment and those with homopolymers longer than 8bp were filtered out. Unique sequences and their frequency in each sample were identified and then a pre-clustering algorithm was used to further de-noise sequences within each sample. Sequences were then chimera checked using UCHIME (Edgar et al., 2011). Reads were then clustered into OTUs at 97% similarity based on uncorrected pairwise distance matrices. OTUs were classified using SILVA reference taxonomy database (release 123, available at http://www.mothur.org/wiki/Silva_reference_files). Chao 1 (species richness), phylogenetic diversity, and Shannon index (species evenness) estimates were generated using mother after normalization to 4000 sequences per sample.

RESULTS

Iron reduction

1° enrichment. Over the first 10 days of incubation, HCl-extractable Fe^{2+} increased from 10 to 25 mM in ferrihydrite treatments (Fig. 1a) and from 10 to 20 mM in goethite treatments (Fig. 1b). From day 6 to 10, HCl-extractable Fe^{3+} (7 and 12 mM in ferrihydrite and goethite treatments, respectively) was completely consumed in all bottles except autoclaved controls with ferrihydrite (data not shown). Iron reduction rates were identical with and without CH_4 (Fig. 1a, b). Initial autoclaving did not suppress Fe^{3+} reduction. A second round of autoclaving on day 6 slightly suppressed further activity. From day 10-28, HCl-extractable Fe^{2+} fluctuated in ferrihydrite treatments (Fig. 1a) and declined slightly in goethite treatments (Fig. 1b). Soluble Fe^{2+} was consistently <1% of HCl-extractable Fe^{2+}, and sediment-free controls did not reduce Fe^{3+} (data not shown).

2° enrichment. After 1:6 dilution and 10 mM ferrihydrite addition on day 50, HCl-extractable Fe^{2+} increased from 3 to 4 mM over the first two days, and then remained constant through the final time point (day 497) in bottles with and without added CH_4 (Fig. 1a). After 10 mM goethite addition on day 50, HCl-extractable Fe^{2+} increased from 2 to 3 mM after a two-day lag period. Thereafter, HCl-extractable Fe^{2+} rose to 4 mM by day 497 in goethite treatments with added CH_4; without CH_4, HCl-extractable Fe^{2+} dropped back to 2 mM (Fig. 1b). Autoclaved controls had no activity. Black magnetic minerals formed in all ferrihydrite treatments except autoclaved controls (Fig 1a). No magnetic minerals formed in goethite treatments (Fig. 1b).

3° enrichment. After 1:10 dilution and addition of 10 mM ferrihydrite on day 352, HCl-extractable Fe^{2+} doubled in the first week in N_2 treatments and bottle CH_4-1 (Fig. 1a). Bottle CH_4-2 displayed similar activity after a two-week lag period. After an additional 100 days, HCl-extractable Fe^{2+} had increased to 2 mM in CH_4 treatments and 1 mM in the N_2 treatment by day 466. Goethite treatments had minimal activity after the first week of 3° enrichment (Fig. 1b).

Autoclaved controls had no activity. As in the 2° enrichment, magnetic minerals formed in the presence of ferrihydrite (Fig. 1a), but not goethite (Fig. 1b).

Methane production

Goethite treatments consistently displayed higher CH_4 production than those with ferrihydrite (Fig. 2). Methanogenesis started during the initial period of Fe^{3+} reduction, and stopped after HCl-extractable Fe^{3+} was completely consumed in the 1° enrichment (day 10). Methanogenesis continued throughout the 3° enrichment. Negligible CH_4 was produced in treatments with ferrihydrite, except for bottle N_2-2 in the 3° enrichment.

Methane oxidation

1° enrichment. ^{13}C incorporation into DIC began on day 6 in both ferrihydrite and goethite treatments and continued throughout the 1° enrichment (Fig. 3a,b). Ferrihydrite treatments showed lower ^{13}C enrichment of the DIC pool but higher total DIC production (totaling to 1.7 and 1.1 μM CH_4 d^{-1} for bottles 1 and 2, respectively) than goethite treatments, which had greatest $\delta^{13}C$ enrichment, but minimal DIC production (0.2 and 0.8 μM CH_4 d^{-1} for bottles 1 and 2, respectively). Autoclaved controls showed neither ^{13}C incorporation nor DIC production.

2° enrichment. Both ferrihydrite treatments displayed ^{13}C enrichment (Fig. 3a), but declined in DIC, precluding calculation of CH_4 oxidation rates. Initial pH of 8 declined to 7.6, 6.7 and 6 in the autoclaved, N_2 and CH_4 treatments, respectively. DIC in goethite treatments with CH_4 dropped to undetectable values within three weeks, suggesting sampling or analytical error, which precluded accurate isotopic measurement at these time points. These data are thus not considered further. Autoclaved and N_2 controls did not show pH changes.

3° enrichment. Bottle CH_4-2 with ferrihydrite was the only treatment with significant ^{13}C incorporation into DIC over the first 15 days (Fig. 3a). DIC also increased over the same interval in both ferrihydrite-amended bottles; calculated CH_4 oxidation rates were 32 and 7 μM d^{-1} in bottle 1 and 2, respectively. The pH dropped from 8.2 to 7.1 and 7.9 in bottles 1 and 2, respectively, over the first 15 days. By day 470, ^{13}C enrichment and DIC concentrations in both ferrihydrite-amended bottles had returned to a level similar to that at the start of the 3° enrichment. Autoclaved controls did not exhibit any change in DIC and pH. Goethite treatments had initial DIC concentrations (3-5 mM) higher than those in previous enrichments. In the goethite-amended autoclaved controls and bottle CH_4-1, DIC concentrations dropped over the 3° enrichment. Only goethite-amended bottle CH_4-2 increased in DIC, without concurrent ^{13}C enrichment.

Microbial taxonomy

Inoculum. 16S rRNA gene amplicons from the sediment inoculum were dominated by those classified as Bathyarchaeota (25%), formerly Miscellaneous Crenarchaeotal Group (MCG; Fig. 4) and unclassified Archaea (11%).

1° enrichment. After 15 days of incubation with Fe^{3+} substrates, species, richness, evenness and phylogenetic diversity decreased relative to the inoculum in all treatments (Fig. 4). Geobacteraceae (Deltaproteobacteria) became dominant (22-36%) in all ferrihydrite treatments (Fig. 4a); the dominant OTU had 97% similarity to *Geothermobacter* sp. Ferrihydrite-amended bottle CH_4-1 was enriched in the Betaproteobacteria, specifically Comamonaceadeae (17%) and Rhodocyclaceae (9%; Fig. 4a). Bathyarchaeota persisted in goethite treatments (11-25%; Fig. 4b).

2° enrichment. By day 72, all treatments had lower species richness, phylogenetic diversity, and evenness. Unclassified Desulfuromondales dominated both ferrihydrite and goethite enrichments (34-68% and 39-53% with ferrihydrite and goethite, respectively). The dominant OTU had 98% similarity to *Geobacter hephaestius.* Bathyarchaeota were depleted compared to the 1° enrichment (Fig. 4). Geobacteraceae declined in ferrihydrite enrichments (2-18%; Fig. 4a). Campylobacteraceae (Epsilonproteobacteria), which was insignificant in the inoculum and the 1° enrichment, comprised 23-40% of sequences in goethite treatments with CH_4; the dominant OTU had 98% similarity to *Sulfurospirillum barnesii* (Fig. 4b). The most abundant methanogenic Euryarchaeota order, Methanobacteriaceae, comprised 1-2% and 6-7% of sequences in ferrihydrite and goethite treatments, respectively the dominant OTU has 100% similarity to *Methanobacterium flexile*.

3° enrichment. By day 469, species richness, phylogenetic diversity, and evenness were even lower than in the 2° enrichment (Fig. 4a,b). Unclassified Desulfuromondales dominated goethite treatments (32-76%; Fig. 4b), but comprised only 18-38% of ferrihydrite treatments. The dominant OTU also had 98% identity to *Geobacter hephaestius/lovleyi*, as in the 2° enrichment. Rhodocyclaceae were more abundant in ferrihydrite treatments with CH_4 (14-15%) than with N_2 (2-4%; Fig 4a); the dominant OTU had 100% similarity to *Azospira oryzae/Dechlorosoma suillum*. Peptococcaceae (Firmicutes) were most abundant in bottle CH_4-2 with ferrihydrite (30%); the dominant OTU had 96% similarity to uncultured members of the genus *Thermincola*. Syntrophaceae (Deltaproteobacteria) were enriched in all ferrihydrite treatments (11-16%) and goethite treatments with N_2 (8-15%); the dominant OTU had 97% similarity to *Smithella propionica*. Methanobacteriaceae comprised 1-4% of sequences in goethite treatments and were

absent from ferrihydrite treatments; as in the 2° enrichment, the dominant OTU had 100% identity to *Methanobacterium flexile*.

DISCUSSION

Rates of Fe^{3+} reduction in long-term ferruginous sediment incubations

Initial rates of HCl-extractable Fe^{2+} production (~1-2 mM d^{-1}) in the 1° enrichment were similar to those from freshwater wetlands (Roden & Wetzel, 2002 ; Jensen et al., 2003 ; Kostka et al., 2002). Activity declined with each successive transfer (0.4 and 0.08 mM d^{-1} for 2° and 3° enrichments, respectively), despite replenishment of Fe^{3+} substrates. Declining Fe^{3+} reduction rates through the incubation period likely reflects limitation by availability of organic carbon, the most thermodynamically favorable electron donor, which was diluted during each successive transfer of the lake sediment. The next two most thermodynamically favorable electron donors are H_2 and CH_4. Hydrogen could have been supplied by fermenters such as Syntrophaceae, but would ultimately still require a source of organic carbon. Methane as an electron donor for microbial Fe^{3+} reduction is thermodynamically favorable and coupling of Fe^{3+} reduction to CH_4 oxidation has been long suspected as a viable microbial metabolism (Caldwell et al., 2008 ; Zehnder & Brock, 1980). In our 2° and 3° enrichments, CH_4 addition resulted in higher Fe^{2+} yield with goethite and ferrihydrite, respectively. This could be the result of (a) methanotrophic growth resulting in production of organics which is used by heterotrophic Fe^{3+} reducers or (b) the direct coupling of CH_4 oxidation and Fe^{3+} reduction. No difference in initial Fe^{2+} production rates however, suggests that initial CH_4 oxidation was driven by another electron donor.

Higher Fe^{3+} reduction rates were maintained on ferrihydrite than goethite, consistent with the higher energetic yield of ferrihydrite vs. goethite as well as its typically greater surface-area.

315 Formation of magnetic minerals was likely due to adsorption of Fe^{2+} onto ferrihydrite followed
316 by solid-state conversion of ferrihydrite to magnetite (Hansel et al., 2003). Since the HCl-
317 extraction method does not dissolve magnetite and magnetite-adsorbed Fe^{2+} (Poulton & Canfield,
318 2005), it is possible that the Fe^{3+} reduction observed in the study is an underestimation of total
319 activity.
320
321 **Fe^{3+} oxide mineralogy controls methane production and methanogen taxonomy**
322 Our observation of higher rates of methanogenesis in goethite vs. ferrihydrite amendments is
323 consistent with prior results showing that bacteria that reduce ferrihydrite better outcompete
324 methanogenic archaea for H_2 and acetate than those that reduce goethite and other more
325 crystalline Fe^{3+} oxides (Lovley & Phillips, 1987 ; Lovley & Goodwin, 1988 ; Zhou et al., 2014 ;
326 Hori et al., 2010 ; Roden & Wetzel, 1996). This outcompetition is also broadly supported by
327 taxonomic shifts. In particular, anaerobic heterotrophs such as *Geothermobacter sp*. (Kashefi et
328 al., 2003) enriched in ferrihydrite treatments by day 15 may have outcompeted other microbes
329 for organic carbon sources.
330 Goethite treatments contained higher abundances of Methanobacteriaceae (0.1-1% and 1-
331 4% on days 15 and 469, respectively) than ferrihydrite treatments (≤0.1% throughout),
332 suggesting that CH_4 in goethite treatments came from the substrates used by
333 Methanobacteriaceae (H_2/CO_2, formate, or CO). The ferrihydrite treatment (bottle 2) that
334 produced CH_4 by day 469 contained 3% Methanosaetaceae, which produce CH_4 from acetate, or
335 from H_2/CO_2 via direct interspecies electron transfer with *Geobacter* (Rotaru et al., 2014). The
336 most dominant OTU had 98% similarity to *Methanosaeta concilii*, in agreement with
337 observations from the Lake Matano water column (Crowe et al., 2011). It is also possible that

archaea could be directly involved in Fe^{3+} reduction (Vargas et al., 1998 ; Sivan et al., 2016), although the lack of methanogenesis in ferrihydrite treatments does not support this.

Fe^{3+}-dependent CH_4 oxidation

Enrichments were established under conditions thought favorable for Fe^{3+}-dependent CH_4 oxidation (e.g. Fe^{3+} oxides and CH_4 as the most abundant electron acceptors and donors, respectively). Incorporation of $^{13}CH_4$ into DIC overlapped with the second phase of Fe^{3+} reduction (days 6-10) in the 1° enrichment but continued after Fe^{3+} reduction stopped at day 10, suggesting an alternative electron acceptor for CH_4 oxidation. Moreover, the stoichiometry of CH_4 oxidized to Fe^{2+} reduced in the 1° enrichment was significantly lower than predicted (1:8; Fig. 5). Low to negative rates of DIC production in the 2° enrichment complicated measurements of CH_4 oxidation. In the 3° enrichment, significant DIC production and ^{13}C incorporation was observed in the first 15 days in bottle CH_4-2 with ferrihydrite, but thereafter isotopic values returned to background levels. The apparent spike in CH_4 oxidation was unlikely coupled to Fe^{3+} reduction (Fig. 5). However, over the same time period, bottle CH_4-1 oxidized methane and reduced iron in a ratio close to the 1 CH_4 oxidized: 8 Fe^{3+} reduced predicted for Fe-AOM (Fig. 5). Goethite-amended cultures were also close to the 1:8 line, albeit with extremely low CH_4 oxidation and Fe^{3+} reduction rates. By the end of 3° enrichment (day 466), CH_4-amended treatments produced twice as much HCl-extractable Fe^{2+} as N_2 treatments, suggesting that Fe^{3+} reduction was stimulated by CH_4. However, without evidence for CH_4 oxidation data during this time interval, we cannot attribute this stimulation to Fe-AOM. It is important to note that these CH_4 oxidation rates may be underestimates due to the low levels of DIC production in our experiments. This suggests that high levels of autotrophy or CO_2 reduction to CH_4 may have

been taking place in our enrichments. In addition, decreasing pH values in some of our enrichments could have pulled DIC into headspace CO_2 subsequently lowering DIC concentrations.

Only minor community composition differences were observed between CH_4- and N_2-cultures; by day 469, the only taxon that was more abundant in the CH_4 vs. N_2 treatments was the betaproteobacterium *Azospira oryzae/Dechlorosoma suillum*, a member of the Rhodocyclaceae family. The potential role of this microbe in CH_4 cycling remains unclear, as laboratory cultures of this species are not known to oxidize CH_4. It is also possible that the growth of novel organisms capable of high rates of Fe^{3+}-dependent CH_4 oxidation was inhibited by other unidentified factors, potentially related to the batch-style incubations, the use of butyl rubber stoppers (Niemann et al., 2015), or the lack of a critical substrate in the enrichment medium.

Effect of Fe^{3+} oxide and carbon substrates on microbial community diversity

The microbial community underwent multiple shifts over the 500-day incubation, with an overall decrease in species richness, species evenness, and phylogenetic diversity over the course of incubation. This was likely in response to declining organic carbon and alternative electron donors. By the 3° enrichment, species evenness was consistently lower in each goethite-amended treatment than in the respective ferrihydrite-amended treatment. This could mean that the greater energetic yield of ferrihydrite reduction fosters higher diversity. Alternatively, the higher reactivity of ferrihydrite may allow it to be utilized by more organisms than goethite.

All of the most enriched taxa have relatives that in laboratory cultures reduce Fe^{3+}. Within those taxa, the most abundant OTUs were closely related to organisms capable of Fe^{3+} reduction (*Geothermobacter sp.*, *Geobacter hephaestius/Geobacter lovleyi*, *Thermincola sp.*, and

384 *Sulfurospirillum barnesii*) (Kashefi et al., 2003 ; Zavarzina et al., 2007 ; Stolz et al., 1999). It is
385 important to note that all taxa enriched in our experiments comprised ≤0.1% of the inoculum
386 community. Desulfuromonadales was the only metal-reducing taxon that was continuously
387 present in all enrichments (3-11%, 34-53%, and 18-76% in the inoculum, 1°, 2°, and 3°
388 enrichment respectively). Other taxa significantly differed in their abundance over the course of
389 incubation. Geobacteraceae was enriched at day 15 with ferrihydrite (22-36%) but had declined
390 in abundance by day 72 (8-18%). Other taxa including Rhodocyclaceae and Peptocaccaceae,
391 were enriched in the presence of ferrihydrite at day 469. In goethite treatments,
392 Campylobacteraceae (23-40%) were enriched at day 72, but did not make up a significant
393 portion of the community at day 469. The succession of different metal-reducing taxa may be
394 due to the changing availability of electron donors (e.g. H_2 and organic C). Enrichment of
395 Syntrophaceae, known for their synthrophic fermentative interactions, suggests the establishment
396 of syntrophy in the 3° enrichment in response to depletion of electron donors.
397
398 **Geobiological implications**
399 The anaerobic microbial metabolisms studied here – Fe^{3+} reduction and hydrogenotrophic
400 methanogenesis – were likely of great importance to the Archean carbon cycle (Konhauser et al.,
401 2005 ; Posth et al., 2013 ; Johnson et al., 2008). The severe organic carbon limitation in our
402 incubations likely mimics conditions of the Archean ocean with relatively low amounts of
403 primary production and biopolymer degradation as well as the absence of complex organic
404 substances supplied by multicellular eukaryotes (Knoll et al., 2016 ; Farquhar et al., 2011). Our
405 results point to a mineralogical control on Fe^{3+}-reduction, methanogenesis, and microbial
406 community composition and diversity. Rapid sedimentation of amorphous Fe^{3+} phases like

ferrihydrite could have supported sediments with diverse communities of Fe^{3+}-reducing organisms that could have outcompeted other taxa such as methanogens for limited carbon and nutrients. Conversely, slow deposition and aging of ferrihydrite to goethite could have limited both the abundance and diversity of Fe^{3+}-reducing organisms, allowing for the establishment of a methanogenic community. Therefore, we posit that methanogenesis rates in the Archean would have depended on the relative abundance of the Fe^{3+} phases and their distributions in marine sediments. Sediments below shallow water columns were likely fed by abundant amorphous Fe^{3+} from photoferrotrophic activity. In the open ocean, organic carbon and Fe^{3+} would have been significantly consumed before reaching sediments, leaving only more crystalline iron phases that are difficult to reduce. Importantly, the role of Fe^{3+}-driven CH_4 oxidation appears limited given our experimental results, though we cannot rule out this pathway given that some of our data suggest it may operate at low rates. Overall, our results support a model for an Archean ferruginous biosphere supported by spatially segregated habitats of bacterial Fe^{3+} reduction from reactive Fe^{3+} oxides, and archaeal methanogenesis in the presence of less reactive Fe^{3+} phases. Rates of Fe deposition, aging, and recrystallization may thus have played an important role in regulating the preservation of sedimentary Fe^{3+}, the production of methane, and the ecology and diversity of the Archean biosphere.

Acknowledgements

This research was funded by NASA Exobiology grant NNX14AJ87G. Support was also provided by a Center for Dark Energy Biosphere Investigations (NSF-CDEBI OCE-0939564) small research grant, and supported by the NASA Astrobiology Institute (NNA15BB03A). SAC was supported through NSERC CRC, CFI, and Discovery grants. We thank Miles Mobley and Johnny Striepen for assistance with laboratory incubations, and Nadia Szeinbaum, Liz Percak-Dennett, Martial Taillefert, and Joel Kostka for helpful discussions.

References

Amos R, Bekins B, Cozzarelli I, Voytek M, Kirshtein J, Jones E, Blowes D (2012) Evidence for iron-mediated anaerobic methane oxidation in a crude oil-contaminated aquifer. *Geobiology,* **10**, 506-517.

Battistuzzi FU, Feijao A, Hedges SB (2004) A genomic timescale of prokaryote evolution: insights into the origin of methanogenesis, phototrophy, and the colonization of land. *BMC Evolutionary Biology,* **4**, 44.

Beal EJ, House CH, Orphan VJ (2009) Manganese- and iron-dependent marine methane oxidation. *Science,* **325**, 184-187.

Brandes JA (2009) Rapid and precise δ13C measurement of dissolved inorganic carbon in natural waters using liquid chromatography coupled to an isotope□ratio mass spectrometer. *Limnology and Oceanography: Methods,* **7**, 730-739.

Caldwell SL, Laidler JR, Brewer EA, Eberly JO, Sandborgh SC, Colwell FS (2008) Anaerobic oxidation of methane: mechanisms, bioenergetics, and the ecology of associated microorganisms. *Environmental science & technology,* **42**, 6791-6799.

Caporaso JG, Lauber CL, Walters WA, Berg-Lyons D, Lozupone CA, Turnbaugh PJ, Fierer N, Knight R (2011) Global patterns of 16S rRNA diversity at a depth of millions of sequences per sample. *Proceedings of the National Academy of Sciences,* **108**, 4516-4522.

Craddock PR, Dauphas N (2011) Iron and carbon isotope evidence for microbial iron respiration throughout the Archean. *Earth and Planetary Science Letters,* **303**, 121-132.

Crowe S, Katsev S, Leslie K, Sturm A, Magen C, Nomosatryo S, Pack M, Kessler J, Reeburgh W, Roberts J (2011) The methane cycle in ferruginous Lake Matano. *Geobiology,* **9**, 61-78.

Crowe S, Roberts J, Weisener C, Fowle D (2007) Alteration of iron□rich lacustrine sediments by dissimilatory iron□reducing bacteria. *Geobiology,* **5**, 63-73.

Crowe SA, Jones C, Katsev S, Magen CD, O'neill AH, Sturm A, Canfield DE, Haffner GD, Mucci A, Sundby BR (2008a) Photoferrotrophs thrive in an Archean Ocean analogue. *Proceedings of the National Academy of Sciences,* **105**, 15938-15943.

Crowe SA, O'neill AH, Katsev S, Hehanussa P, Haffner GD, Sundby B, Mucci A, Fowle DA (2008b) The biogeochemistry of tropical lakes: A case study from Lake Matano, Indonesia. *Limnology Oceangraphy,* **53**, 319-331.

Edgar RC, Haas BJ, Clemente JC, Quince C, Knight R (2011) UCHIME improves sensitivity and speed of chimera detection. *Bioinformatics,* **27**, 2194-2200.

Egger M, Rasigraf O, Sapart CJ, Jilbert T, Jetten MS, Ro□Ckmann T, Van Der Veen C, Ba□Nda□ N, Kartal B, Ettwig KF (2015) Iron-mediated anaerobic oxidation of methane in brackish coastal sediments. *Environmental Science & Technology,* **49**, 277-283.

Farquhar J, Zerkle AL, Bekker A (2011) Geological constraints on the origin of oxygenic photosynthesis. *Photosynthesis Research,* **107**, 11-36.

Fournier GP, Gogarten JP (2008) Evolution of acetoclastic methanogenesis in *Methanosarcina* via horizontal gene transfer from cellulolytic *Clostridia*. *Journal of Bacteriology,* **190**, 1124-1127.

Fu L, Li S-W, Ding Z-W, Ding J, Lu Y-Z, Zeng RJ (2016) Iron reduction in the DAMO/*Shewanella oneidensis* MR-1 coculture system and the fate of Fe(II). *Water Research,* **88**, 808-815.

Hansel CM, Benner SG, Neiss J, Dohnalkova A, Kukkadapu RK, Fendorf S (2003) Secondary mineralization pathways induced by dissimilatory iron reduction of ferrihydrite under advective flow. *Geochimica et Cosmochimica Acta,* **67**, 2977-2992.

Hansen JW, Thamdrup B, Jørgensen BB (2000) Anoxic incubation of sediment in gas-tight plastic bags: a method for biogeochemical process studies. *Marine Ecology Progress Series*, **208**, 273-282.

Haqq-Misra JD, Domagal-Goldman SD, Kasting PJ, Kasting JF (2008) A revised, hazy methane greenhouse for the Archean Earth. *Astrobiology,* **8**, 1127-1137.

Hori T, Müller A, Igarashi Y, Conrad R, Friedrich MW (2010) Identification of iron-reducing microorganisms in anoxic rice paddy soil by 13C-acetate probing. *The ISME journal*, **4**, 267-278.

Jensen MM, Thamdrup B, Rysgaard S, Holmer M, Fossing H (2003) Rates and regulation of microbial iron reduction in sediments of the Baltic-North Sea transition. *Biogeochemistry,* **65**, 295-317.

Johnson CM, Beard BL, Roden EE (2008) The iron isotope fingerprints of redox and biogeochemical cycling in modern and ancient Earth. *Annual Reviews of Earth and Planetary Sciences,* **36**, 457-493.

Kappler A, Pasquero C, Konhauser KO, Newman DK (2005) Deposition of banded iron formations by anoxygenic phototrophic Fe(II)-oxidizing bacteria. *Geology*, **33**, 865-868.

Kashefi K, Holmes DE, Baross JA, Lovley DR (2003) Thermophily in the Geobacteraceae: Geothermobacter ehrlichii gen. nov., sp. nov., a Novel Thermophilic Member of the Geobacteraceae from the "Bag City" Hydrothermal Vent. *Applied and Environmental Microbiology,* **69**, 2985-2993.

Kasting JF (2005) Methane and climate during the Precambrian era. *Precambrian Research* **137**, 119-129.

Knoll AH, Bergmann KD, Strauss JV (2016) Life: the first two billion years. *Phil. Trans. R. Soc. B*, **371**, 20150493.

Konhauser K, Newman D, Kappler A (2005) The potential significance of microbial Fe(III) reduction during deposition of Precambrian banded iron formations. *Geobiology*, **3**, 167-177.

Kostka JE, Luther GW (1994) Partitioning and speciation of solid phase iron in saltmarsh sediments. *Geochemica Cosmochimica Acta*, **58**, 1701-1710.

Kostka JE, Roychoudhury A, Van Cappellen P (2002) Rates and controls of anaerobic microbial respiration across spatial and temporal gradients in saltmarsh sediments. *Biogeochemistry*, **60**, 49-76.

Kozich JJ, Westcott SL, Baxter NT, Highlander SK, Schloss PD (2013) Development of a dual-index sequencing strategy and curation pipeline for analyzing amplicon sequence data on the MiSeq Illumina sequencing platform. *Applied and environmental microbiology*, **79**, 5112-5120.

Lovley D, Phillips E (1986) Organic matter mineralization with reduction of ferric iron in anaerobic sediments. *Applied and Environmental Microbiology*, **51**, 683-689.

Lovley DR, Goodwin S (1988) Hydrogen concentrations as an indicator of the predominant terminal electron-accepting reactions in aquatic sediments. *Geochimica et Cosmochimica Acta*, **52**, 2993-3003.

Lovley DR, Phillips EJ (1987) Competitive mechanisms for inhibition of sulfate reduction and methane production in the zone of ferric iron reduction in sediments. *Applied and Environmental Microbiology*, **53**, 2636-2641.

Niemann H, Steinle L, Blees J, Bussmann I, Treude T, Krause S, Elvert M, Lehmann MF (2015) Toxic effects of lab-grade butyl rubber stoppers on aerobic methane oxidation. *Limnology and Oceanography: Methods*, **13**, 40-52.

Noroi KA, Thamdrup B, Schubert CJ (2013) Anaerobic oxidation of methane in an iron-rich Danish freshwater lake sediment. *Limnology and oceanography*, **58**, 546-554.

Pavlov AA, Kasting JF, Brown LL, Rages KA, Freedman R (2000) Greenhouse warming by CH4 in the atmosphere of early Earth. *Journal of Geophysical Research: Planets*, **105**, 11981-11990.

Posth NR, Konhauser KO, Kappler A (2013) Microbiological processes in banded iron formation deposition. *Sedimentology*, **60**, 1733-1754.

Poulton SW, Canfield DE (2005) Development of a sequential extraction procedure for iron: implications for iron partitioning in continentally derived particulates. *Chemical Geology*, **214**, 209-221.

Poulton SW, Canfield DE (2011) Ferruginous conditions: a dominant feature of the ocean through Earth's history. *Elements*, **7**, 107-112.

Riedinger N, Formolo M, Lyons T, Henkel S, Beck A, Kasten S (2014) An inorganic geochemical argument for coupled anaerobic oxidation of methane and iron reduction in marine sediments. *Geobiology*, **12**, 172-181.

Roden EE, Wetzel RG (1996) Organic carbon oxidation and suppression of methane production by microbial Fe (III) oxide reduction in vegetated and unvegetated freshwater wetland sediments. *Limnology and Oceanography*, **41**, 1733-1748.

Roden EE, Wetzel RG (2002) Kinetics of microbial Fe (III) oxide reduction in freshwater wetland sediments. *Limnology and Oceanography*, **47**, 198-211.

Rooze J, Egger M, Tsandev I, Slomp CP (2016) Iron□dependent anaerobic oxidation of methane in coastal surface sediments: Potential controls and impact. *Limnology and Oceanography*.

Rotaru A-E, Shrestha PM, Liu F, Shrestha M, Shrestha D, Embree M, Zengler K, Wardman C, Nevina KP, Lovley DR (2014) A new model for electron flow during anaerobic digestion: direct interspecies electron transfer to Methanosaeta for the reduction of carbon dioxide to methane. *Energy & Environmental Science*, **7**, 408-415.

Scheller S, Yi H, Chadwick GL, Mcglynn SE, Orphan VJ (2016) Artificial electron acceptors decouple archaeal methane oxidation from sulfate reduction. *Science*, **351**, 703-707.

Schloss PD, Westcott SL, Ryabin T, Hall JR, Hartmann M, Hollister EB, Lesniewski RA, Oakley BB, Parks DH, Robinson CJ (2009) Introducing mothur: open-source, platform-independent, community-supported software for describing and comparing microbial communities. *Applied and environmental microbiology*, **75**, 7537-7541.

Segarra KEA, Comerford C, Slaughter J, Joye SB (2013) Impact of electron acceptor availability on the anaerobic oxidation of methane in coastal freshwater and brackish wetland sediments. *Geochimica et Cosmochimica Acta*, **115**, 15-30.

Sivan O, Adler M, Pearson A, Gelman F, Bar-Or I, John SG, Eckert W (2011) Geochemical evidence for iron-mediated anaerobic oxidation of methane. *Limnology and Oceanography*, **56**, 1536-1544.

Sivan O, Antler G, Turchyn AV, Marlow JJ, Orphan VJ (2014) Iron oxides stimulate sulfate-driven anaerobic methane oxidation in seeps. *Proceedings of the National Academy of Sciences*, **111**, 4139-4147.

Sivan O, Shusta SS, Valentine DL (2016) Methanogens rapidly transition from methane production to iron reduction. *Geobiology*, **DOI: 10.1111/gbi.12172**.

Stolz JF, Ellis DJ, Blum JS, Ahmann D, Lovley DR, Oremland RS (1999) Note: Sulfurospirillum barnesii sp. nov. and Sulfurospirillum arsenophilum sp. nov., new members of the

572 Sulfurospirillum clade of the ε-Proteobacteria. *International Journal of Systematic and*
573 *Evolutionary Microbiology*, **49**, 1177-1180.

574 Stookey LL (1970) Ferrozine---a new spectrophotometric reagent for iron. *Analytical Chemistry*,
575 **42**, 779-781.

576 Sturm A, Fowle DA, Jones C, Leslie KL, Nomosatryo S, Henny C, Canfield DE, Crowe S
577 (2015) Rates and pathways of methane oxidation in ferruginous Lake Matano, Indonesia.
578 *Biogeosciences Discussions*, **12**, 1-34.

579 Ueno Y, Yamada K, Yoshida N, Maruyama S, Isozaki Y (2006) Evidence from fluid inclusions
580 for microbial methanogenesis in the early Archaean era. *Nature*, **440**, 516-519.

581 Vargas M, Kashefi K, Blunt-Harris EL, Lovley DR (1998) Microbiological evidence for Fe(III)
582 reduction on early Earth. *Nature*, **395**, 65-67.

583 Zavarzina DG, Sokolova TG, Tourova TP, Chernyh NA, Kostrikina NA, Bonch-Osmolovskaya
584 EA (2007) Thermincola ferriacetica sp. nov., a new anaerobic, thermophilic, facultatively
585 chemolithoautotrophic bacterium capable of dissimilatory Fe(III) reduction.
586 *Extremophiles*, **11**, 1-7.

587 Zehnder AJ, Brock TD (1980) Anaerobic methane oxidation: occurrence and ecology. *Applied*
588 *and Environmental Microbiology*, **39**, 194-204.

589 Zhou S, Xu J, Yang G, Zhuang L (2014) Methanogenesis affected by the co-occurrence of iron
590 (III) oxides and humic substances. *FEMS Microbiology Ecology*, **88**, 107-120.

591

592

593

594

595

596

597

598

Figure Captions

Figure 1. HCl-extractable Fe^{2+} for sediment enrichments with (a) ferrihydrite and (b) goethite over 497 days. Timeline at top shows transfer dates and dilution ratios. "A" represents days that controls were autoclaved. Red and black symbols represent treatments with and without CH_4, respectively. White symbols represent autoclaved controls. All treatments were run in duplicate (circle and triangle symbols). Tertiary enrichments are magnified as inset. Photos depict 2° and 3° enrichment bottles on day 497 with evidence for magnetic mineral formation in live treatments amended with ferrihydrite.

Figure 2. Accumulation of CH_4 in the headspace of sediment enrichments. Timeline at top shows transfer dates and dilution ratios. Solid and dotted lines represent ferrihydrite and goethite treatments, respectively. All treatments were run in duplicate (circle and triangle symbols). Original headspace was 100% N_2.

Figure 3. Dissolved inorganic carbon (DIC) isotopic composition and concentration for sediment enrichments amended with $^{13}CH_4$ and either (a,c) ferrihydrite or (b,d) goethite. Timeline at top shows transfer dates and dilution ratios. "A" represents days that controls were autoclaved. Red and white symbols represent live treatments and autoclaved controls, respectively. Errors bars represent standard deviation of triplicate measurements. Calculated methane oxidation rates for the 1° enrichment were 1.7 and 1.1 μM CH_4 d^{-1} ferrihydrite bottles 1 and 2, respectively and 0.2 and 0.8 μM CH_4 d^{-1} for goethite bottles 1 and 2, respectively. Isotopic data are not plotted for DIC concentrations 0.5 mM. Rate calculations were not possible for the 2° enrichment due to low/variable DIC.

620 **Figure 4. 16S rRNA gene diversity and phylogenetic diversity for inoculum and sediment**
621 **enrichments amended with (a) ferrihydrite and (b) goethite.** Samples were taken on day 15
622 (1° enrichment), 72 (2° enrichment) and 469 (3° enrichment). Red and black symbols represent
623 treatments with and without CH_4, respectively. Gray diamonds represent inoculum samples. All
624 treatments were run in duplicate (circle and triangle symbols). Species richness, phylogenetic
625 diversity, and species evenness for the sediment inoculum and enrichments normalized to 4000
626 sequences per sample are shown to the right of barcharts.

627 **Figure 5. Rates of HCl-extractable Fe^{3+} reduction rates vs. CH_4 production (black symbols)**
628 **or CH_4 oxidation (red symbols).** Autoclaved controls are white circles. "F" indicates
629 ferrihydrite and "G" indicates goethite. The red line indicates the line for the predicted ratio of 1
630 mol CH_4 oxidized per 8 mol Fe^{3+} reduced. Tertiary enrichments are magnified as inset.

631

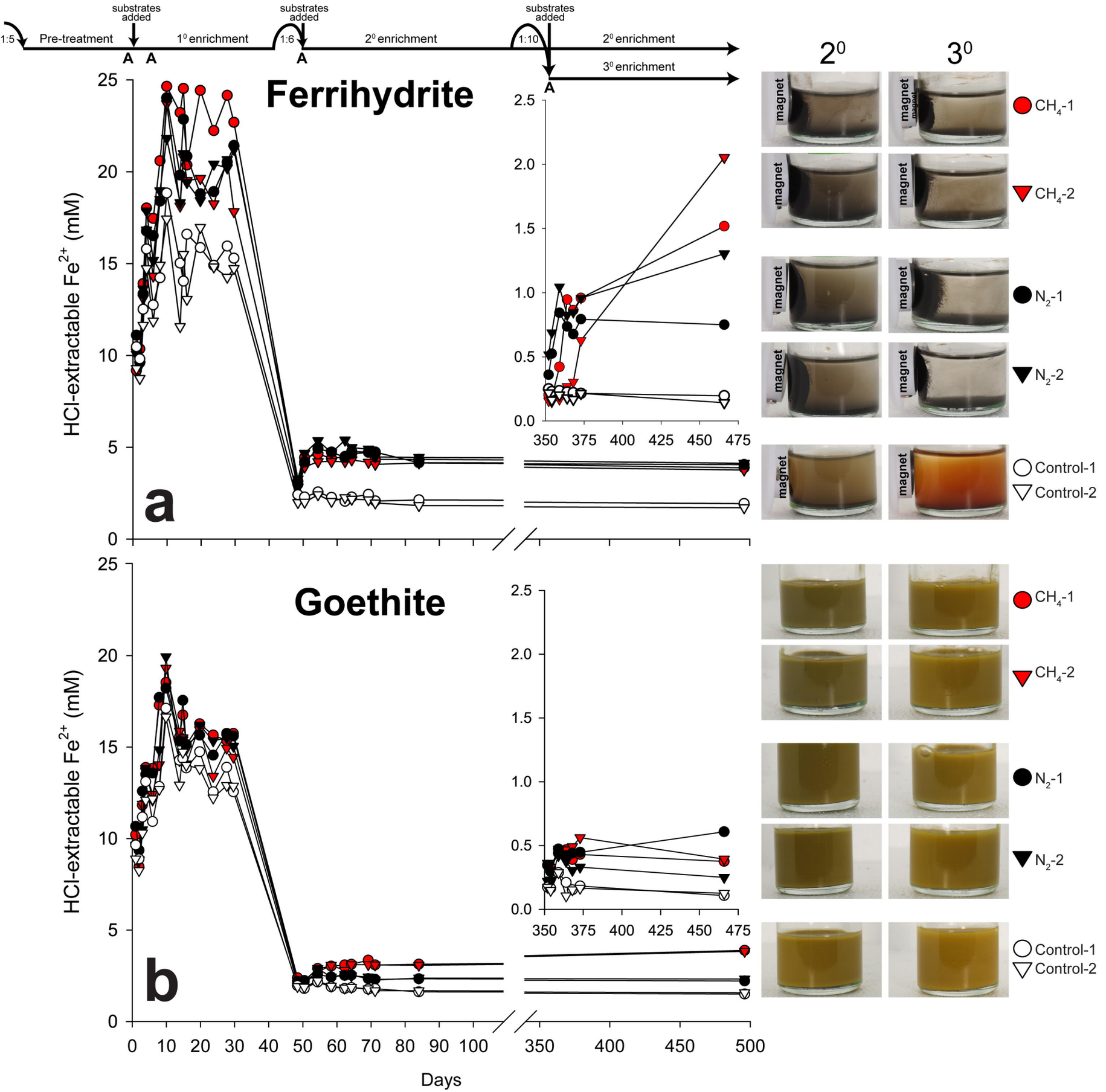
substrates added
1:5
Pre-treatment
1⁰ enrichment
1:6
2⁰ enrichment
1:10
2⁰ enrichment
3⁰ enrichment
A
Ferrihydrite
HCl-extractable Fe2+ (mM)
a
Goethite
b
Days
2⁰
3⁰
magnet
CH4-1
CH4-2
N2-1
N2-2
Control-1
Control-2

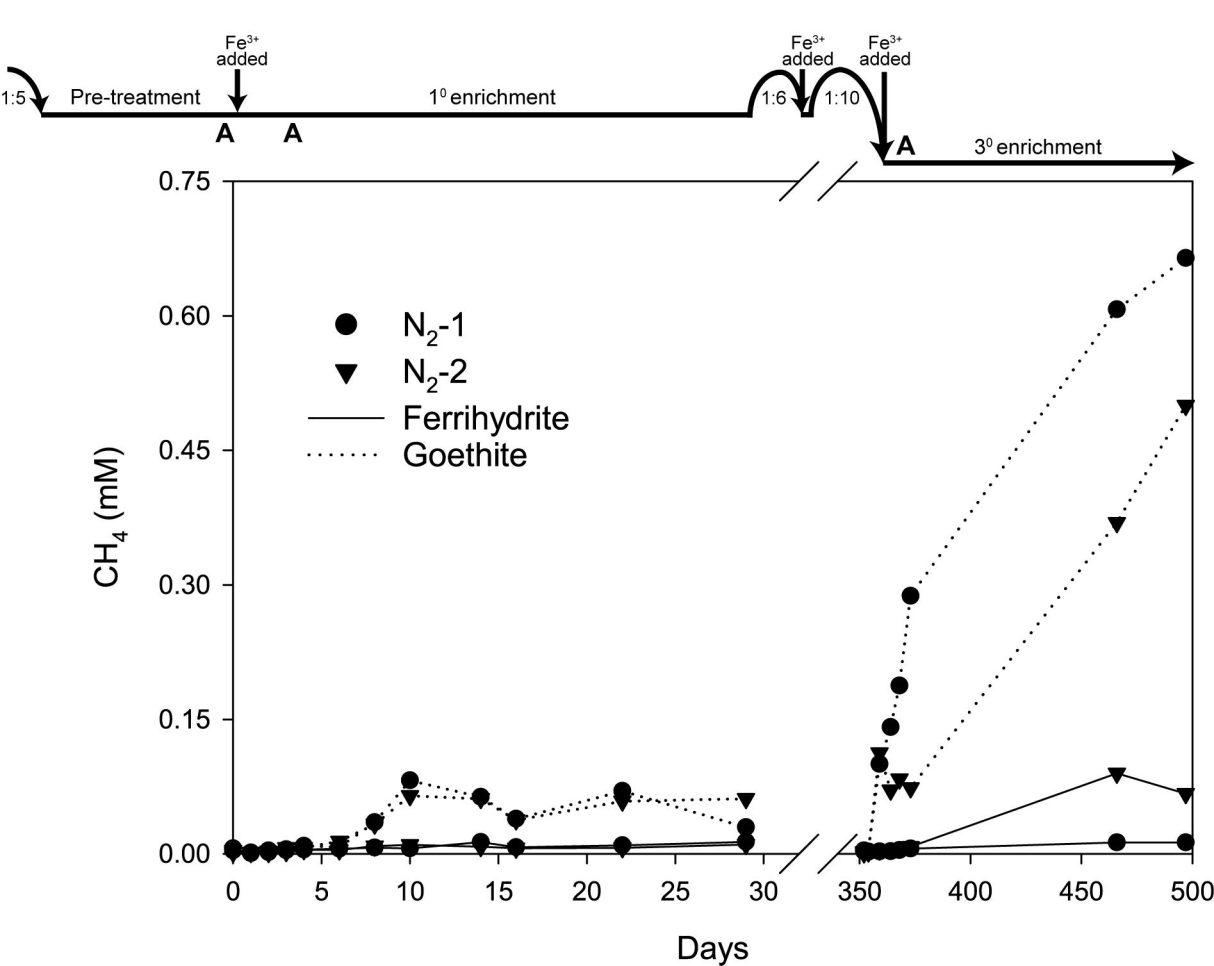
Fe3+ added
1:5
Pre-treatment
1⁰ enrichment
A
A
Fe3+ added
1:6
Fe3+ added
1:10
A
3⁰ enrichment
0.75
0.60
0.45
0.30
0.15
0.00
CH4 (mM)
N2-1
N2-2
Ferrihydrite
Goethite
0
5
10
15
20
25
30
350
400
450
500
Days

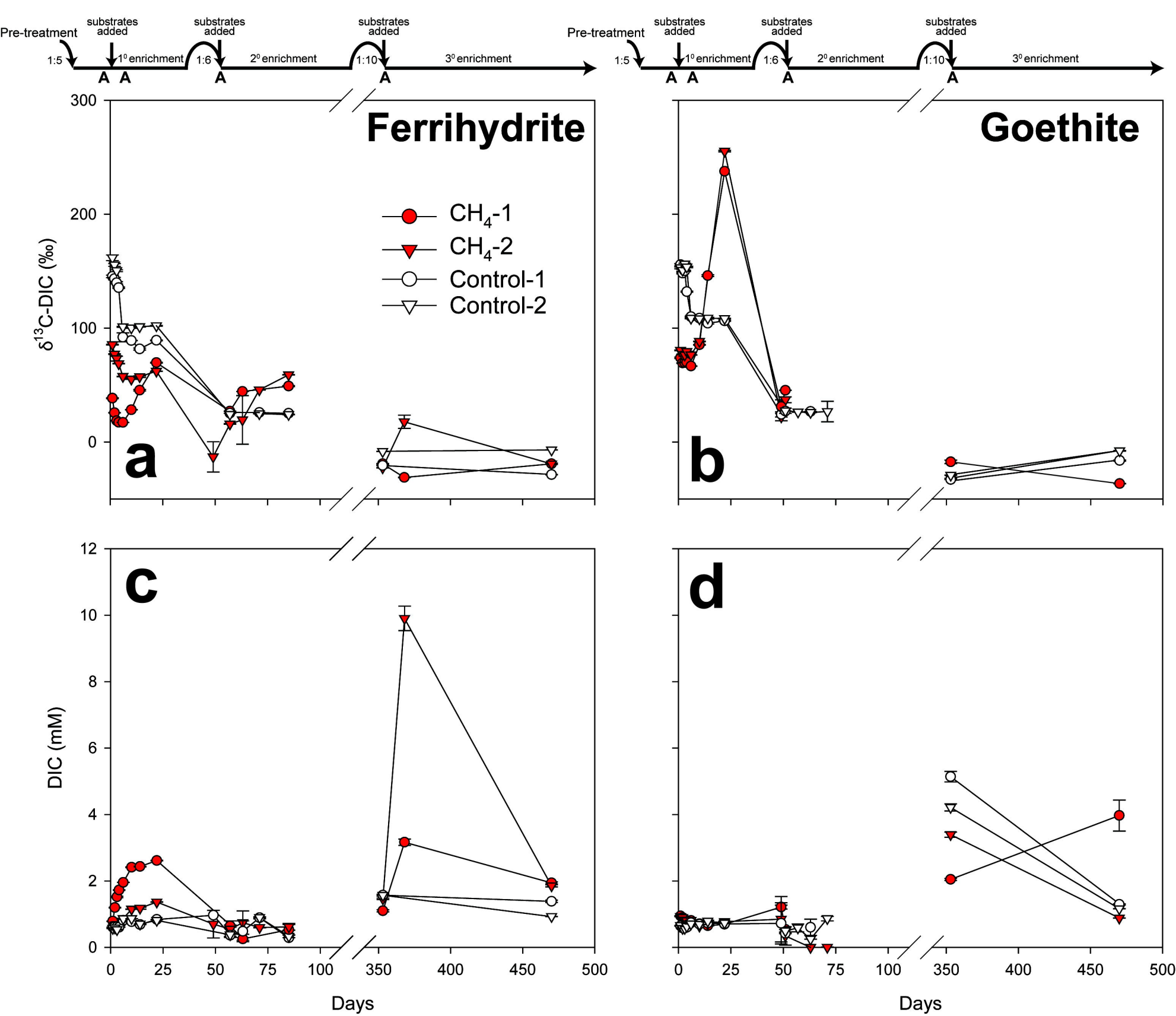
Pre-treatment
substrates added
1:5
1⁰ enrichment
1:6
2⁰ enrichment
1:10
3⁰ enrichment
A
Ferrihydrite
Goethite
CH4-1
CH4-2
Control-1
Control-2
δ13C-DIC (‰)
DIC (mM)
a
b
c
d
Days

Ferrihydrite

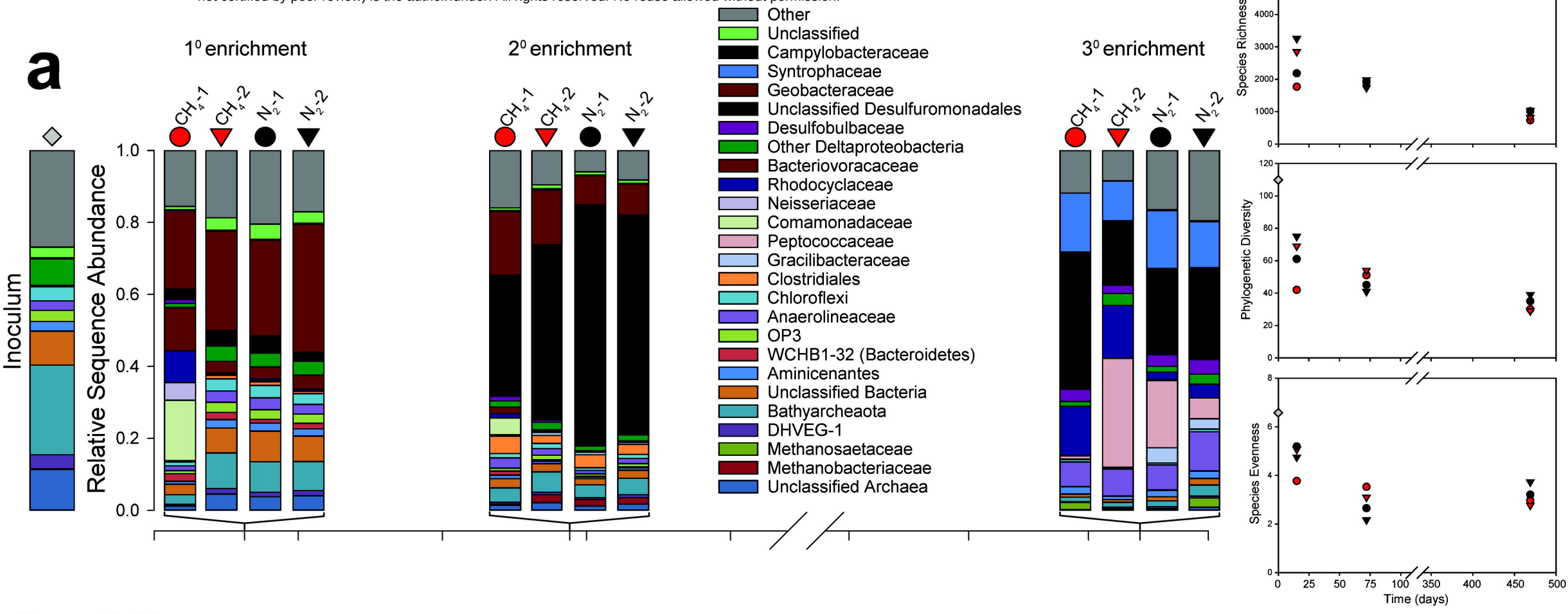

Goethite

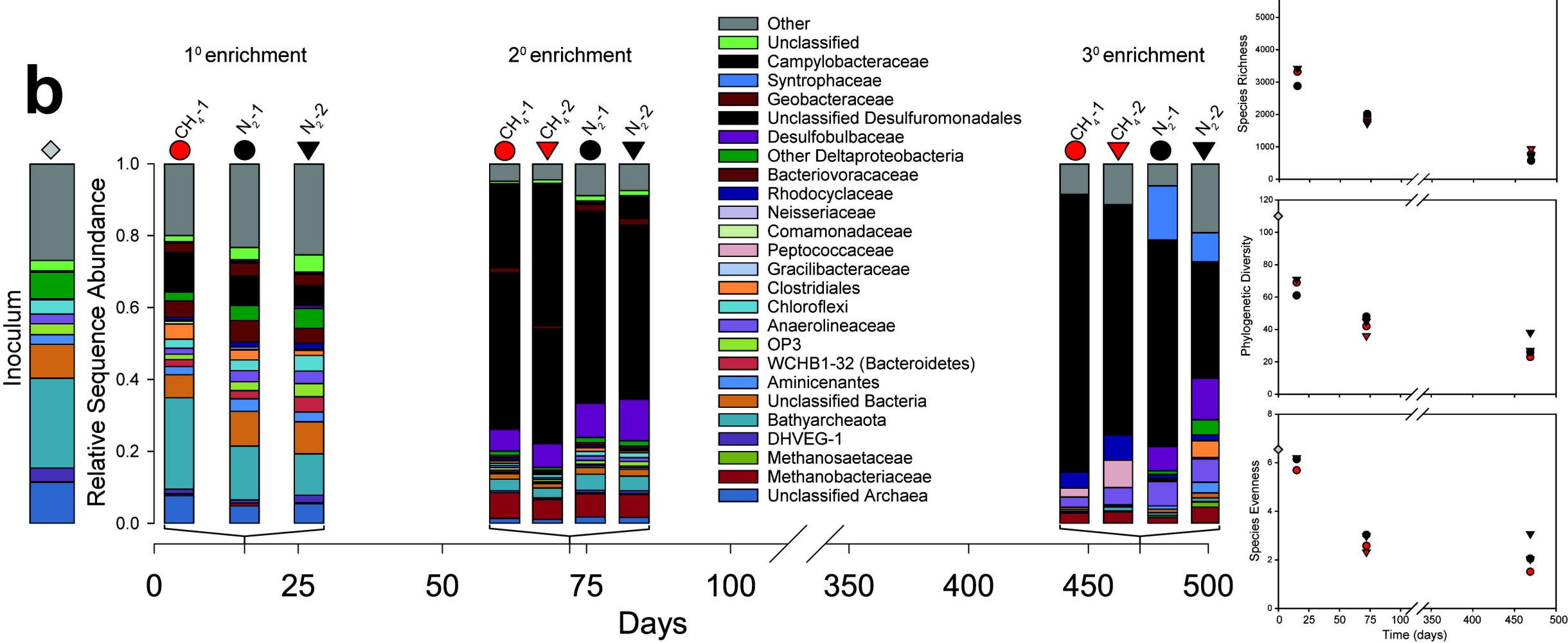

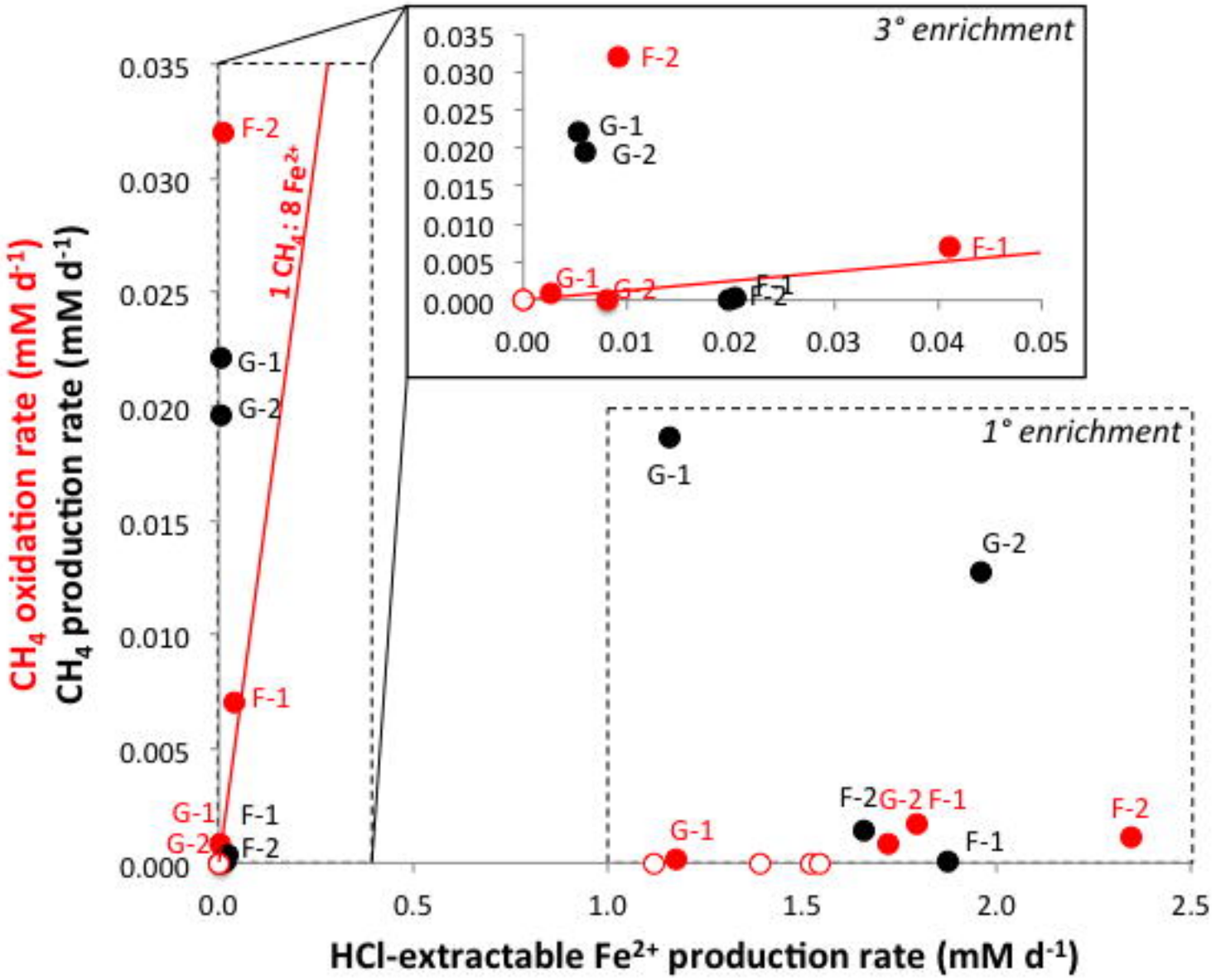
3° enrichment
1° enrichment
1 CH4 : 8 Fe2+
F-2
G-1
G-2
F-1
CH4 oxidation rate (mM d-1)
CH4 production rate (mM d-1)
HCl-extractable Fe2+ production rate (mM d-1)
0.000
0.005
0.010
0.015
0.020
0.025
0.030
0.035
0.0
0.5
1.0
1.5
2.0
2.5
0.00
0.01
0.02
0.03
0.04
0.05